Supplementary Materials

Stable hexaazatrinaphthylene-based covalent organic framework as high-capacity electrodes for aqueous hybrid supercapacitors

Xu Li[1,2], Zhenhu Li[1,3,*], Yulin Zhang[1,3], Hanlin Guo[4], Meiying Zou[1,3], Haoxiang Li[1,3], Yuping Liu[1,3], Shuangyi Liu[1,3,*]

[1]Research Center for Electrochemical Energy Storage Technologies, Chongqing Institute of Green and Intelligent Technology, Chinese Academy of Sciences, Chongqing 400714, China.

[2]Chongqing CAS Supercap Technology Co., Ltd., Chongqing 401329, China.

[3]Chongqing School, University of Chinese Academy of Sciences, Chongqing 400714, China.

[4]School of Physics and Electronic Engineering, Harbin Normal University, Harbin 150025, Heilogjiang, China.

[*]**Correspondence to:** Dr. Zhenhu Li and Prof. Shuangyi Liu, Research Center for Electrochemical Energy Storage Technologies, Chongqing Institute of Green and Intelligent Technology, Chinese Academy of Sciences, 266 Fangzheng Avenue, Chongqing 400714, China. E-mail: lizhenhu@cigit.ac.cn; liushuangyi@cigit.ac.cn

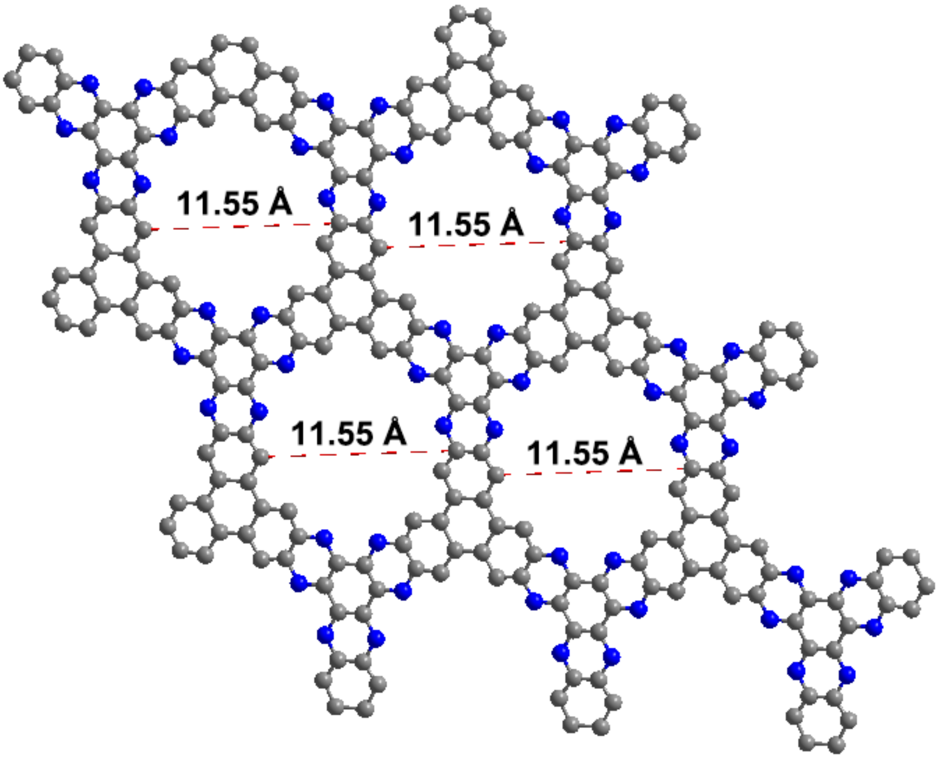

Figure S1. Simulated pore diameter of HATN-COF.

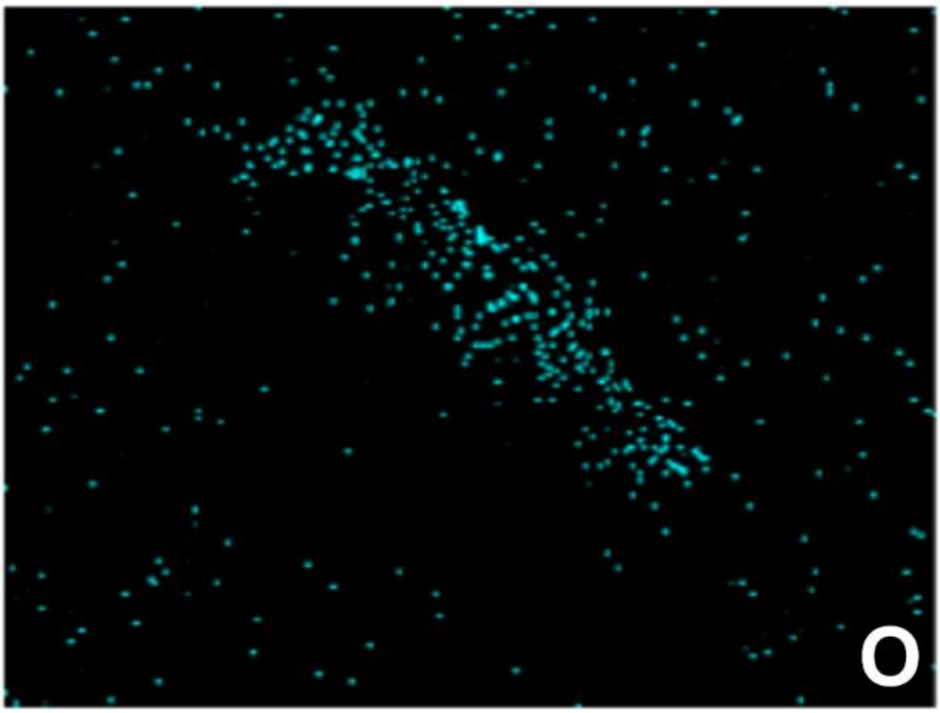

Figure S2. EDS elemental mapping of O element in the HATN-CO.

Table S1. Elemental analysis of C and N contents of HATN-COF by a Vario EL cube analyzer

Element	Atomic percent (%)	Atomic ratio
C	71.5	3.4
N	20.9	1
H	7.6	-

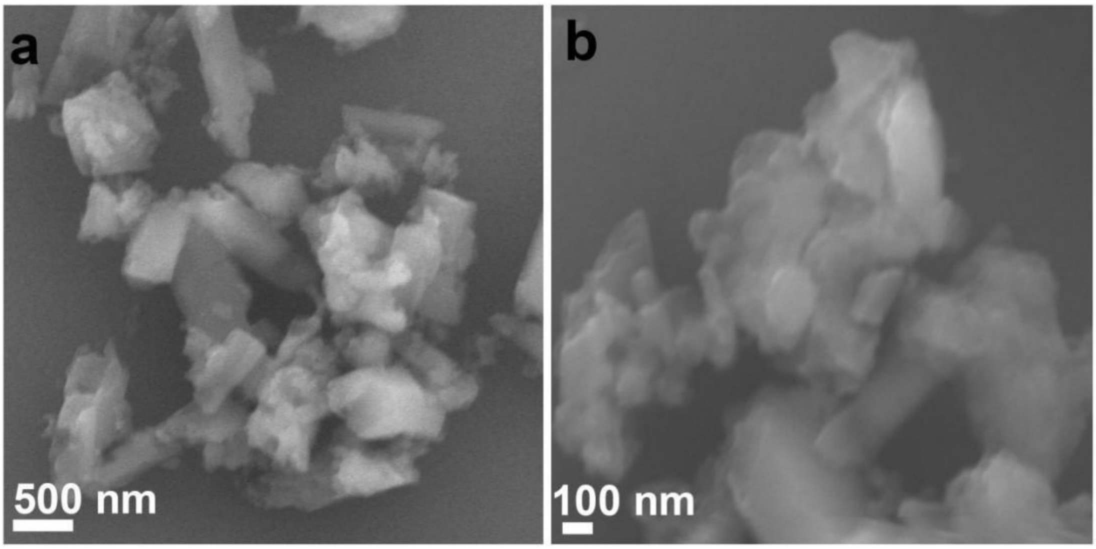

Figure S3. SEM images at different magnification after ultrasonic crushing of HATN-COF.

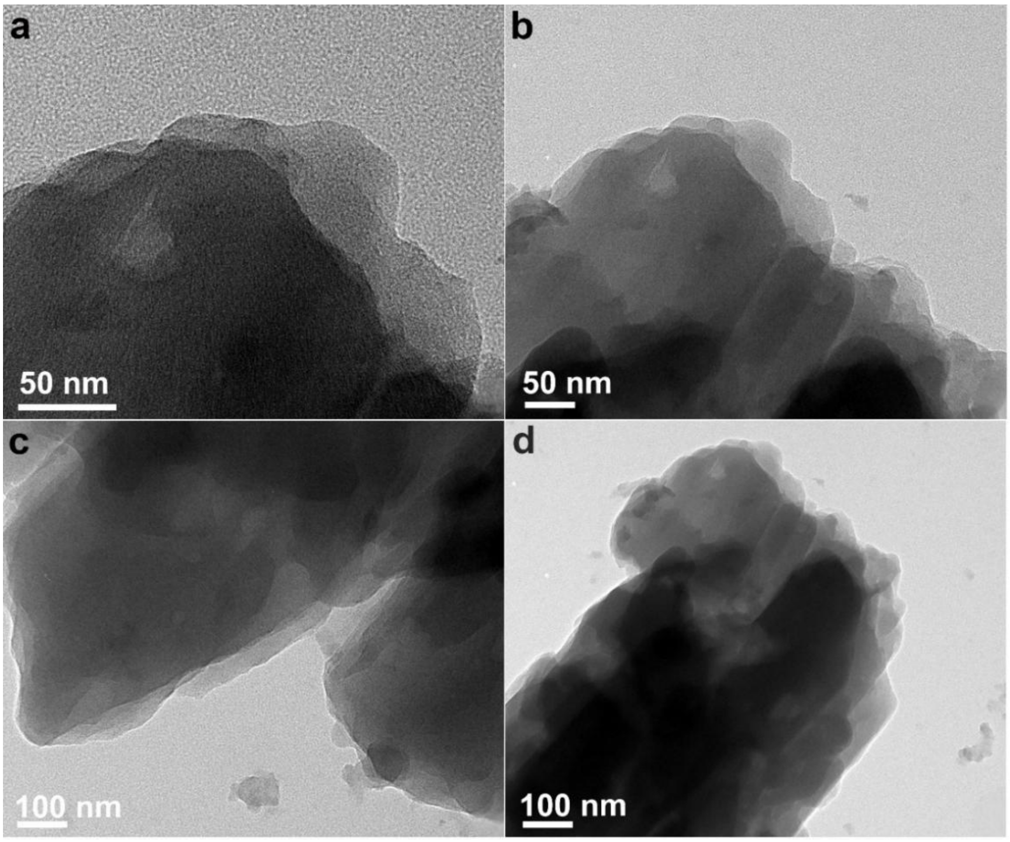

Figure S4. TEM images of HATN-COF.

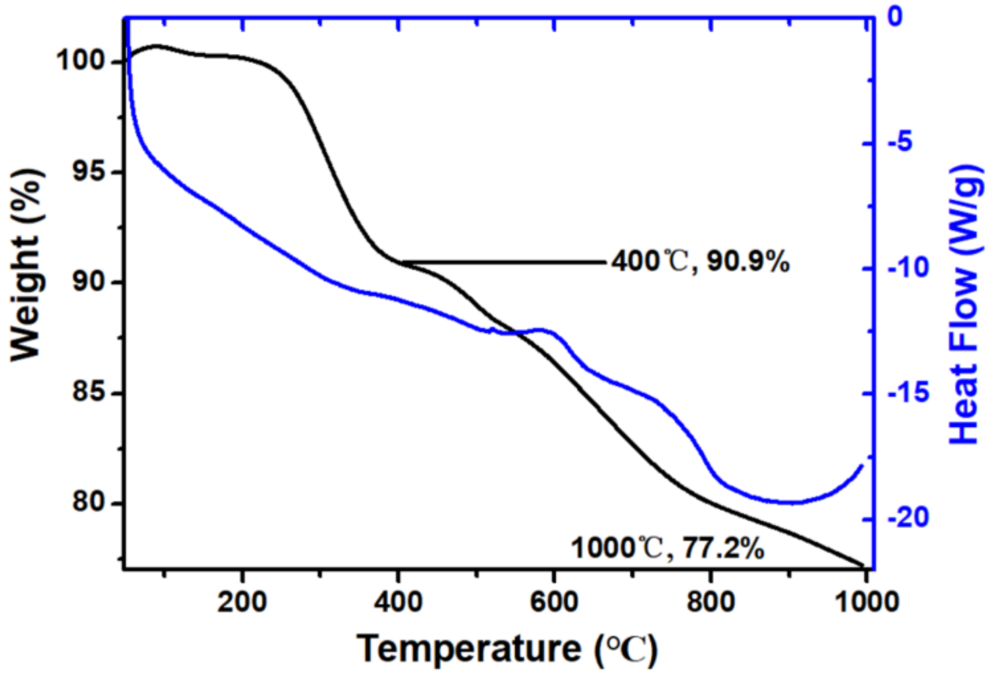

Figure S5. TGA-DSC curves of HATN-COF.

The thermostability of HATN-COF is estimated by using the thermogravimetric analysis (TGA). The TGA curve can be divided into two stages between room temperature and 1000°C. A 9.1% weight loss below 400°C resulted from the adsorbed and crystalline ethanol and water molecules of the interlayer of HATN-COF. Approximately 13.7% weight loss between 401 and 1000°C attributing to sectional collapse of organic ligands. The result indicates that HATN-COF remains high thermostability at the range from room temperature to 400°C.

Table S2. The C, N and O contents of HATN-COF by XPS spectra

Element	Atomic percent (%)
C	74.8
N	15.7
O	9.4

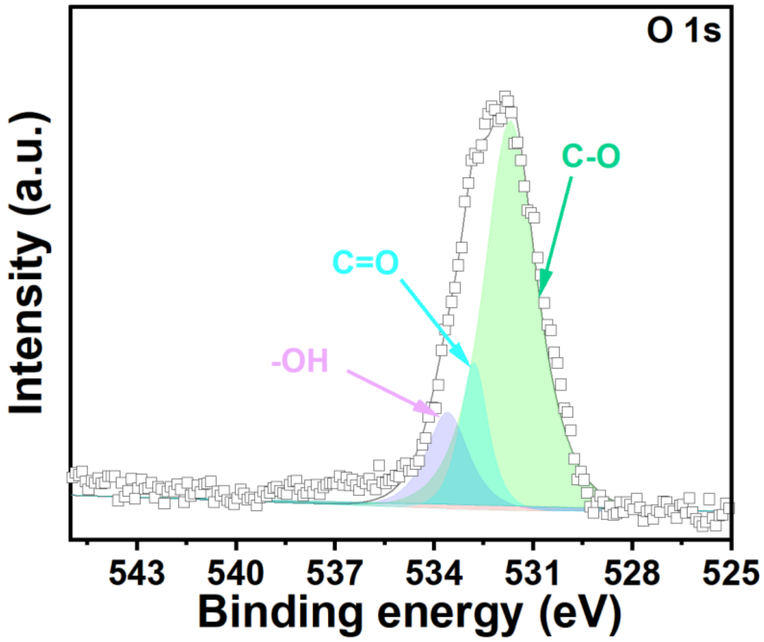

Figure S6. The high resolution XPS spectrum of O 1s of HATN-COF.

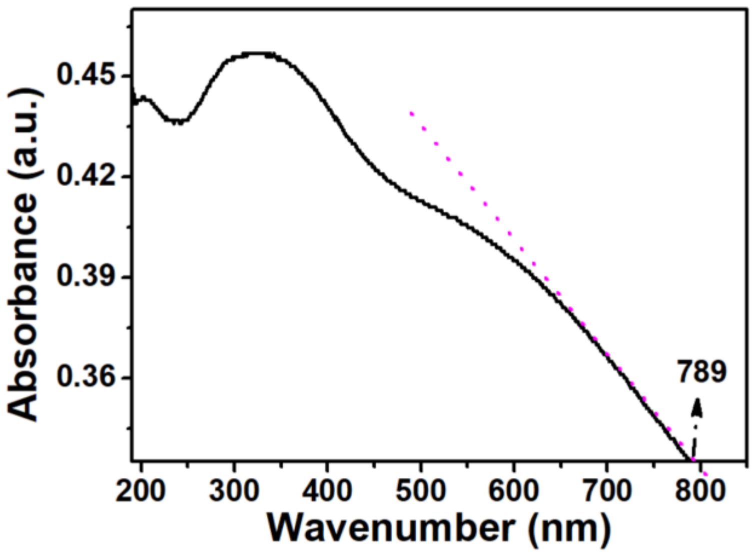

Figure S7. The UV-Vis spectrum of HATN-COF.

The optical band gap is determined to be 1.6 eV, corresponding to a maximum absorption wavelength of 789 nm (the intersection of the purple dotted line and the X-axis in Figure. S6), indicative of semiconductor behavior[1], according to the formula:

$$Eg^{op} = hv = (1240/\lambda_{abs})\ \text{eV} \qquad (1)$$

where Eg^{op} is the optical band gap energy (eV), $h = 6.626196\times10^{-34}$ J·s, v is the frequency (Hz), and λ is the maximum absorption wavelength (nm).

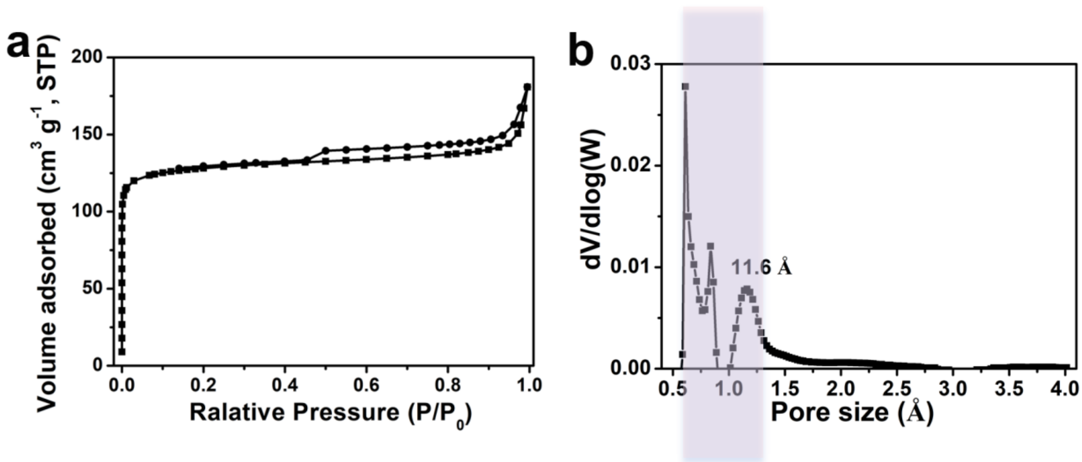

Figure S8. (a) Nitrogen adsorption-desorption isotherm curves and (b) pore size distribution curve of HATN-COF.

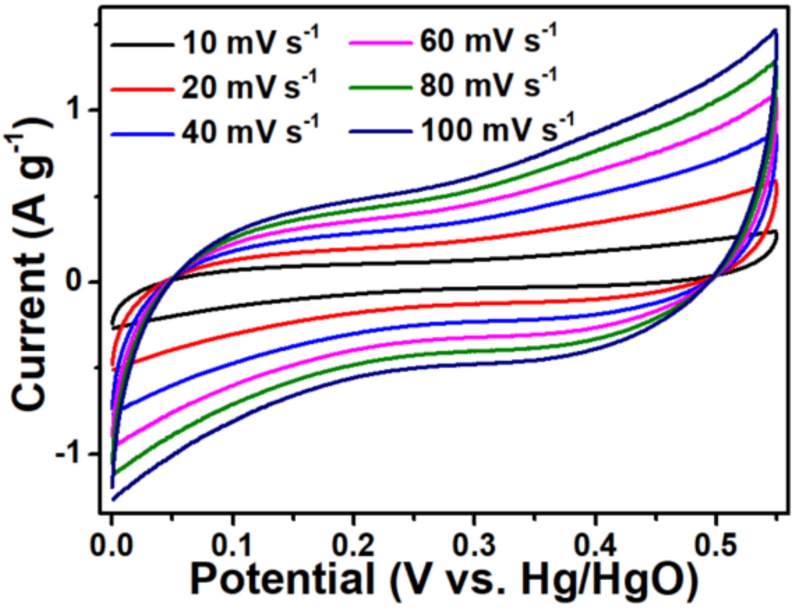

Figure S9. CV curves of HATN-COF electrode from 10 to 100 mV s^{-1} in 1M Na_2SO_4 electrolyte.

The specific capacitance is 18.6 F g^{-1} at 10 mV s^{-1} in the neutral 1M Na_2SO_4 electrolyte.

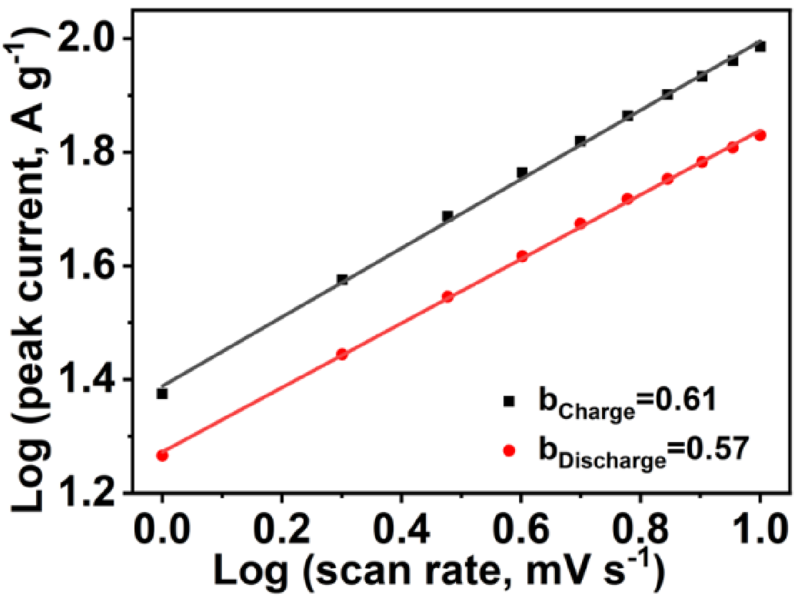

Figure S10. Normalized peak-current plot to determine the *b* value for anodic process of HATN-COF electrode.

Table S3. Specific capacity of HATN-COF electrode from 1 to 20 A g^{-1}

Current density (A g^{-1})	Specific capacity (mAhg^{-1})
1	367.3
2	364.6
4	355.0
6	351.8
8	330.1
10	313.2
20	259.7

Table S4. COF-based electrode material and their electrochemical performance in three-electrode system reported in literature

Electrode	Specific capacitance	Electrolyte	Retention (Cycles)	References
Ni-COF	1257 F g^{-1} at 1 A g^{-1}	3 M KOH	94% (10,000)	[2]
Phos-COF-1	100 F g^{-1} at 1 A g^{-1}	3 M Na_2SO_4	90% (5000)	[3]
PT-COF	1443 F g^{-1} at 1 A g^{-1}	0.5 M H_2SO_4	91% (3000)	[4]
TpOMe-DAQ	169 F g^{-1} at 3.3 mA cm^{-2}	3 M H_2SO_4	65% (50,000)	[5]
COF@OHP@CNTF	249 F g^{-1} at 30 mV s^{-1}	1 M H_3PO_4	80% (10,000)	[6]
N-PC	112 F g^{-1} at 1 A g^{-1}	6 M KOH	88.4% (5000)	[7]
Ppy@COF	1983 mF g^{-1} at 1 A g^{-1}	1 M PVA-H_2SO_4	98% (2800)	[8]
HATN-COF	367.3 mAhg^{-1} (2644.5 F g^{-1}) at 1 A g^{-1}	6 M KOH	97.8% (20,000)	This work

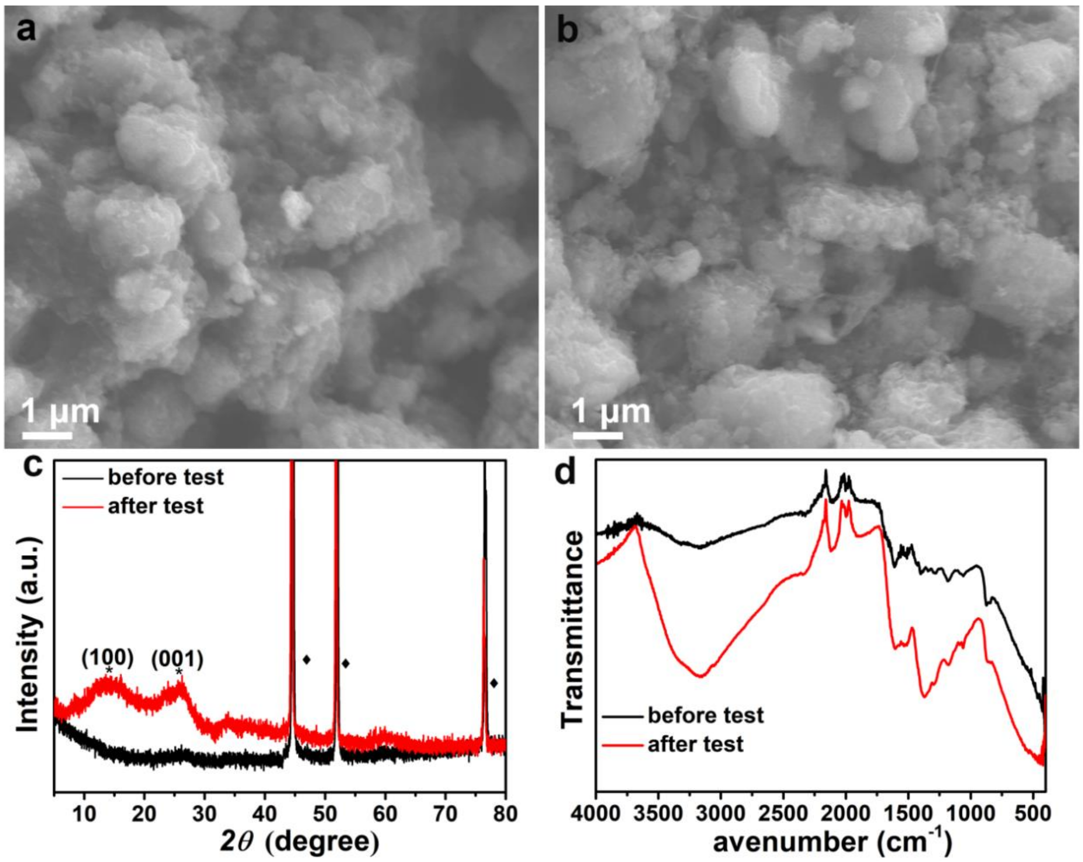

Figure S11. Structure and morphology characterizations of HATN-COF electrode. SEM images of (a) before and (b) after the cycling test at 6 A g^{-1}. (c) XRD patterns of before and after the cycling test at 6 A g^{-1}, Note that the peaks marked with * and ♦ originate from HATN-COF and nickel foam, respectively. (d) FTIR spectra of before and after the cycling test at 6 A g^{-1}.

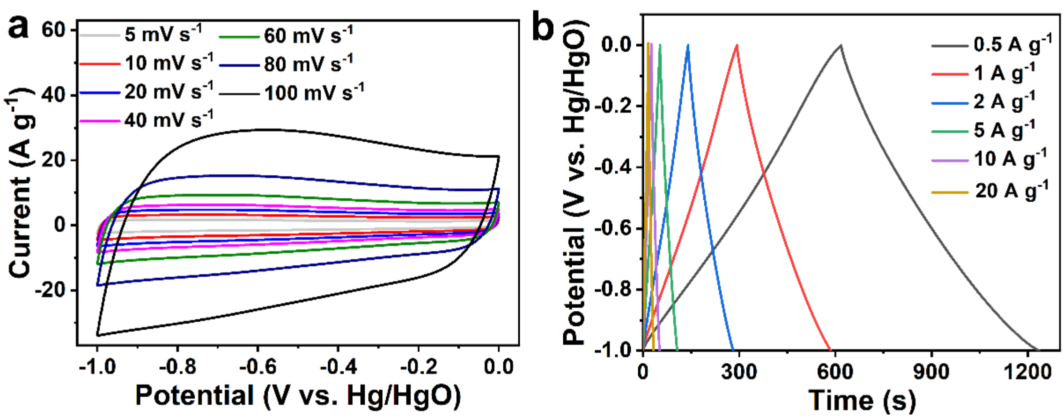

Figure S12. Electrochemical performances of AC electrode. (a) CV curves at different scan rates. (b) GCD curves at different current densities.

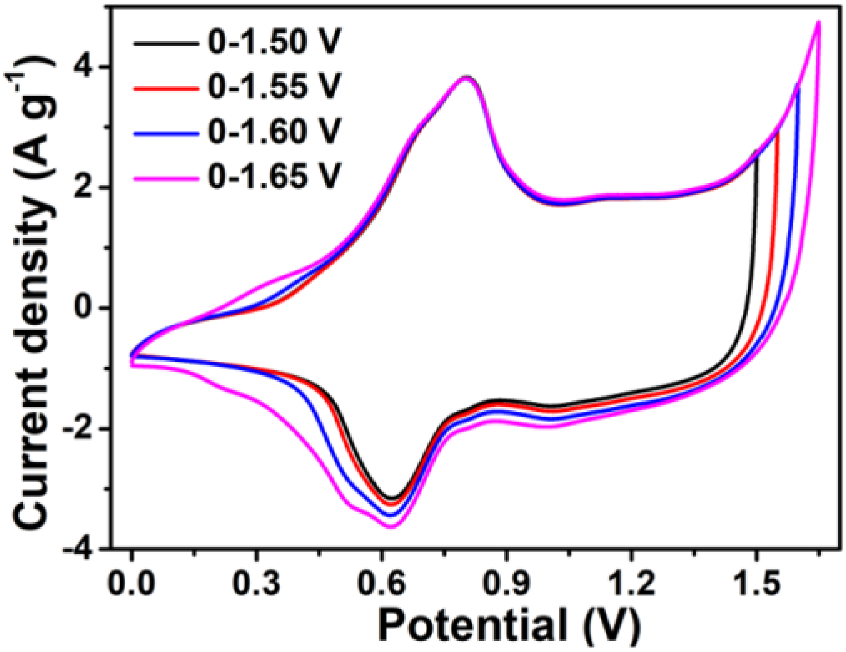

Figure S13. CV curves of HATN-COF//AC at various voltage windows.

Table S5. COF-based electrode material and their electrochemical performance in two-electrode system reported in literature

Electrode	Specific capacitance ($F\ g^{-1}$)	Retention (Cycles)	Energy density at power density	References
PI-COF//PI-COF	163 $F\ g^{-1}$ at 0.5 $A\ g^{-1}$	84.1% (30,000)	35.7 $W\ h\ kg^{-1}$ at 250 $W\ kg^{-1}$	[9]
$[C_{60}]$0.05COF//rGO	47.6 $F\ g^{-1}$ at 1 $A\ g^{-1}$	99% (5000)	21.4 $W\ h\ kg^{-1}$ at 900 $W\ kg^{-1}$	[10]
FCTF//AC	148 $F\ g^{-1}$ at 1 $A\ g^{-1}$	98.9% (10,000)	46.3 $W\ h\ kg^{-1}$ at 975 $W\ kg^{-1}$	[11]
RuO_2//Hex-COF	64 $F\ g^{-1}$ at 1 $A\ g^{-1}$	89% (7500)	23.3 $W\ h\ kg^{-1}$ at 661.2 $W\ kg^{-1}$	[12]
TpTa-Py //TpTa-Py	102 $F\ g^{-1}$ at 0.5 $A\ g^{-1}$	92% (6000)	9.06 $W\ h\ kg^{-1}$ at 100 $W\ kg^{-1}$	[13]

PFM-COF1//PFM-COF1	158 F g^{-1} at 0.5 A g^{-1}	81% (2000)	28.44 W h kg^{-1} at 1077.72 W kg^{-1}	[14]
PDC MA COF//AC	94 F g^{-1} at 1 A g^{-1}	88% (20,000)	29.2 W h kg^{-1} at 750 W kg^{-1}	[15]
HATN-COF//AC	215.4 F g^{-1} at 0.5 A g^{-1}	97.3% (20,000)	67.3 W h kg^{-1} at 375 W kg^{-1}	This work

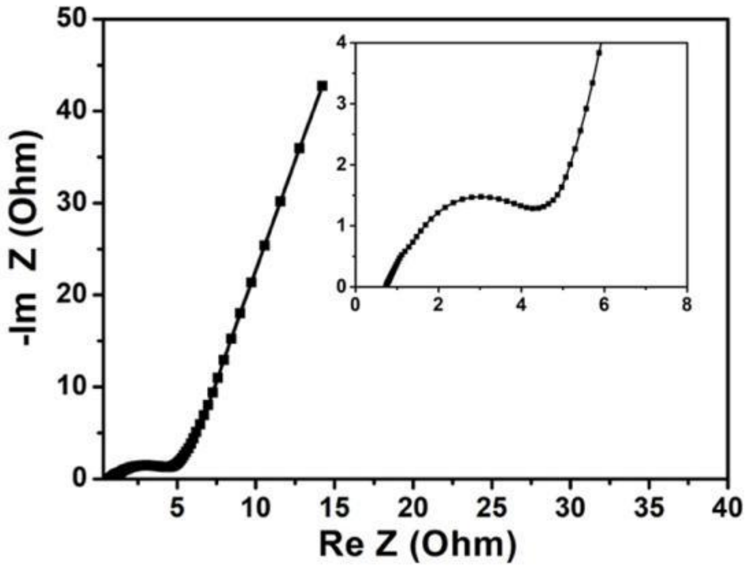

Figure S14. Nyquist plots, with the inset showing the enlarged portion of HATN-COF//AC.

References

1 Iqbal R, Majeed MK, Hussain A et al. Boosting the Crystallinity of Novel Two-Dimensional Hexamine Dipyrazino Quinoxaline-Based Covalent Organic Frameworks for Electrical Double-Layer Supercapacitors. *Micropor Mesopor Mat* 2023;7:2464-2474. DOI:10.1039/D3QM00169E

2 Li T, Zhang WD, Liu Y et al. A Two-Dimensional Semiconducting Covalent Organic Framework with Nickel(Ⅱ) Coordination for High Capacitive Performance. *J Mater Chem A* 2019;7:19676-19681. DOI:10.1039/c9ta07194f

3 Sajjad M, Tao R, Qiu L. Phosphine Based Covalent Organic Framework as an Advanced Electrode Material for Electrochemical Energy Storage. *J Mater Sci-mater El* 2021;32:1602-1615. DOI:10.1007/s10854-020-04929-9

4 Patra BC, Bhattacharya S. New Covalent Organic Square Lattice Based on Porphyrin and Tetraphenyl Ethylene Building Blocks toward High-Performance Supercapacitive Energy Storage. *Chem Mater* 2021;33:8512-8523. DOI:10.1021/acs.chemmater.1c02973

5 Halder A, Ghosh M, Khayum MA et al. Interlayer Hydrogen-Bonded Covalent Organic Frameworks as High-Performance Supercapacitors. *J Am Chem Soc* 2018;140:10941-10945. DOI:10.1021/jacs.8b06460

6 Xu Z, Liu Y, Wu Z et al. Construction of Extensible and Flexible Supercapacitors from Covalent Organic Framework Composite Membrane Electrode. *Chem Eng J* 2020;387:124071. DOI:10.1016/j.cej.2020.124071

7 Vargheese S, Dinesh M, Kavya KV, Pattappan D, Rajendra Kumar RT, Haldorai Y. Triazine-Based 2D Covalent Organic Framework-Derived Nitrogen-Doped Porous Carbon for Supercapacitor Electrode. *Carbon Lett* 2021;31:879-886. DOI:10.1007/s42823-020-00190-6

8 Haldar S, Rase D, Shekhar P et al. Vaidhyanathan R, Incorporating Conducting Polypyrrole into a Polyimide Cof for Carbon-Free Ultra-High Energy Supercapacitor. *Adv Energy Mater* 2022;12:2200754. DOI:10.1002/aenm.202200754

9 Iqbal R, Badshah A, Ma YJ, Zhi LJ. An Electrochemically Stable 2D Covalent Organic Framework for High-Performance Organic Supercapacitors. *Chinese J Polym Sci* 2020;38:558-564. DOI:10.1007/s10118-020-2412-z

10 Zhao X, Sajjad M, Zheng Y et al. Covalent Organic Framework Templated Ordered Nanoporous C_{60} as Stable Energy Efficient Supercapacitor Electrode Material. *Carbon* 2021;182:144-154. DOI:10.1016/j.carbon.2021.05.061

11 Gao Y, Zhi C, Cui P, Zhang KAI, Lv LP, Wang Y. Halogen-Functionalized Triazine-Based Organic Frameworks Towards High Performance Supercapacitors. *Chem Eng J* 2020;400:125967. DOI:10.1016/j.cej.2020.125967

12 Kandambeth S, Jia J, Wu H et al. Covalent Organic Frameworks as Negative Electrodes for High-Performance Asymmetric Supercapacitors. *Adv Energy Mater* 2020;10:202001673. DOI:10.1002/aenm.202001673

13 Khattak AM, Ghazi ZA, Liang B et al. A Redox-Active 2D Covalent Organic Framework with Pyridine Moieties Capable of Faradaic Energy Storage. *J Mater Chem A* 2016;4:16312-16317. DOI:10.1039/C6TA05784E

14 Biradar MR, Rao CRK, Bhosale SV, Bhosale SV. Flame-Retardant 3D Covalent Organic Framework for High-Performance Symmetric Supercapacitors. *Energy Fuels* 2023;37:4671-4681. DOI:10.1021/acs.energyfuels.2c04226

15 Li L, Lu F, Xue R et al. Ultrastable Triazine-Based Covalent Organic Framework with an Interlayer Hydrogen Bonding for Supercapacitor Applications. *ACS Appl Mater Interfaces* 2019;11:26355-26363. DOI:10.1021/acsami.9b06867